6.0 NATURAL HYDROPHOBIC RESPONSE SCHEME AND FAVORABLE KINETICS FOR PCB CF FROTH FLOTATION

6.1 INTRODUCTION

Results of the investigations based on the natural hydrophobic response scheme are presented and discussed in this chapter. Useful inferences made from the preliminary microflotation are mentioned first. The variations in response – mass pull, extent of fit to first order kinetic, assay and recovery – with the kinetic regimes employed serve both to: assess a favourable kinetic regime for PCB fines flotation; as well as for drawing a conclusion on the applicability of froth flotation, and the natural hydrophobic response scheme, in particular, in concentrating the PCB comminution fines.

6.2 PRELIMINARY MICROFLOTATION

During the microflotation experiments, it was observed that 130 rpm (1.8 lpm) peristaltic pump setting, commonly used for mineral microflotation investigations (Bradshaw and O'Connor, 1996), produced high turbulence in the cell column. The particles were carried through to the top of the suspension and the quiescent zone could not be observed. The pump setting had to be lowered to 40 rpm. It was observed that even 10 rpm would still maintain suspension of the pulp after aeration. This low energy input required to keep the particles in suspension is understandable, given the low bulk density of the sample and the large -38 µm proportion (Section 5.2). This observation informed the choice of the low range of initial impeller speeds used for the flotation investigation in the Leeds cells (see Section 4.5).

The detailed observation of the pulp pH over time is shown in Figure 6.1, which indicated that the natural pulp pH averages around 8.00. It also shows that the natural pulp pH is acceptably stable with time and a variation of pH over the flotation period will not occur. This observation and clarification is necessary given the diversity of the sample constituents, where the possibility of slow dissolution of acids or bases may not be ruled out without a definite confirmation.

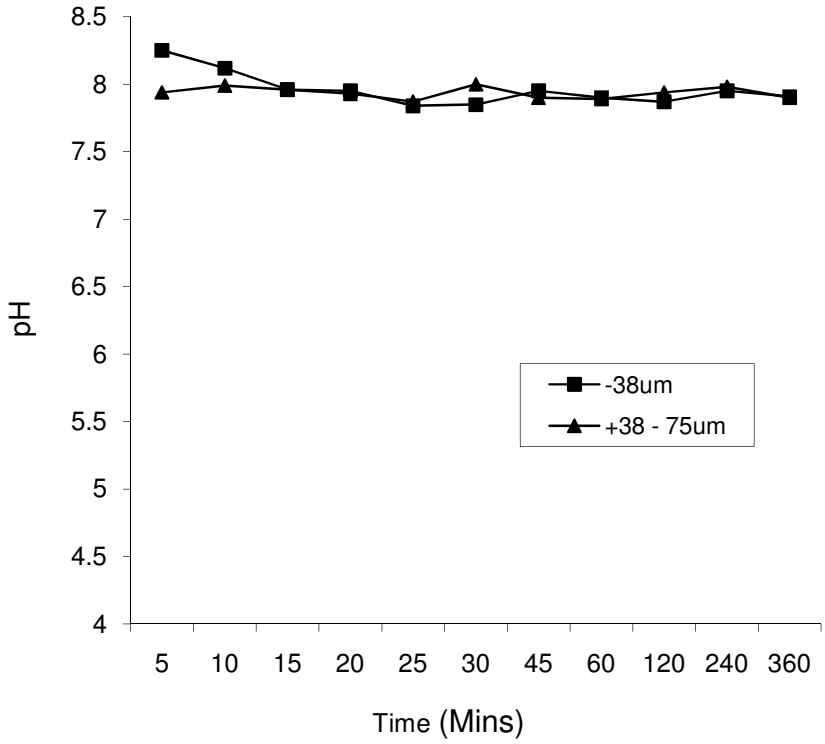

Figure 6.1: Natural pulp pH with time for two size fractions

Figure 6.2 shows mass pull data that summarises major observation from the microflotation treatments. The initial treatment using a collector pulled a fraction of the sample well above 50 wt %. This fraction being so high reinforced the idea of particles floating under natural hydrophobic response. This was confirmed, as flotation without any treatment also gave high mass pulls. A further observation was that mass pull does not tend to be higher when a collector is used compared to when it is not. At 200 g/ton dosage, the mass pull even appeared to be lowered (Figure 6.2). When a collector was used with detergent as a wetting agent (designated CWA in Figure 6.2), a remarkable drop in the mass pull was observed.

Basically, the detergent acted as an ionic surfactant and lowered the surface tension of the pulp. It follows that the collectorless mass pull is due to particles floating under their natural hydrophobicity, and that when the pulp surface tension was reduced certain particles were wetted and remained in the sink. Collectors as surfactants also generally contribute some decrease in the liquid surface tension (Section 3.2). This may explain some decrease in the mass pull that seems to accompany the SIBX conditioning compared to the collectorless flotation. The distinct

collectorless response observed encouraged detailed investigations into the prospect of the natural hydrophobic response described in Section 3.5.1. The scheme was simultaneously used for studying the favorable kinetics for PCB CF flotation.

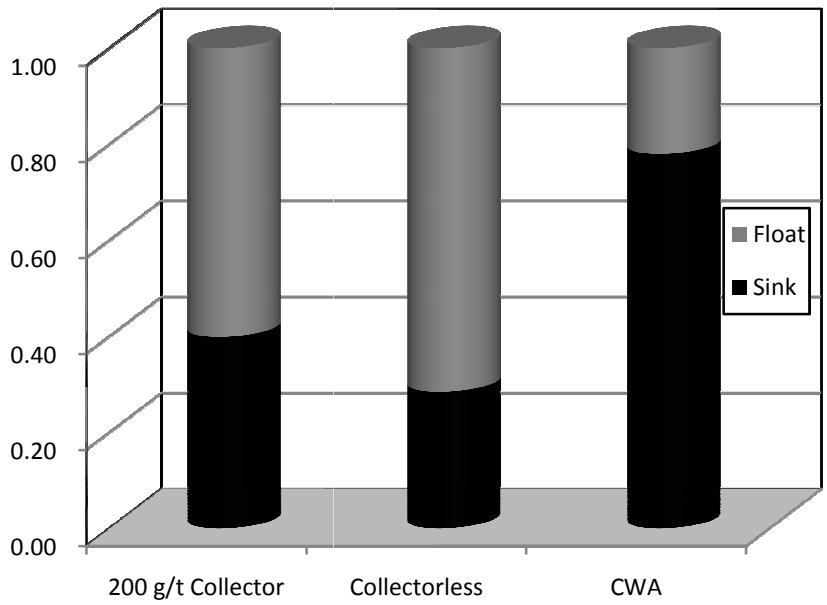

Figure 6.2: Microflotation float and sink fractions represented in stacked columns scaled to a total of 1.

6.3 THE NATURAL HYDROPHOBIC RESPONSE SCHEME

6.3.1 The Natural Hydrophobic Froth

As observed previously, without the addition of any reagent, the pulp pH measurements in the Leeds cell averaged 8.00 (δr = 1.6%) for measurement in 14 different pulps. Also, for all the kinetic conditions investigated, and without any frother addition, stable froths formed in the cell. Figure 6.3 shows a picture of the froth build-up inside the cell (see also Appendix 2.2). This distinctly shows that the natural hydrophobic response exists. The observed mass pull was also generally high, above 50% in most conditions (see Section 6.3.2).

Figure 6.3: PCB CF froth in the flotation cell under natural hydrophobic response

This immediately clarifies the difficulty experienced in pulping the sample. Despite the fact that the true density should sink the particles, the bulk hydrophobic behaviour kept water out, so that the sample formed into globules covered by a skin of water. The particles inside the globules remained dry, retaining the loose bulk density (see Section 5.2). The globules thus easily floated on top of the pulp. Intense agitation simply broke the globules into smaller sizes, while aerating the pulp at the same time. A scum thus formed on top of the pulp, even before commencement of flotation. This is a frustration of the operation, as the scum contains tiny globules with trapped dry sample inside, which does not allow separation of the sink constituent. The way around this was to form a paste of the sample first, introduce it to the cell, cover the paste with water and then break the paste under the water with the impeller. This is summarised as a peculiarity of this sample which demands that pulping must be done under water.

Considering the extent of frothing observed as indicated in Figure 6.3, another issue that needs to be addressed is the origin of this froth. A possible assumption is for an inherent frothing constituent in the heterogeneous sample. Exploring this assumption, an inventory of organics present in the sample shows that none of the thermoplastic constituents, PVC, ABS, PET, etc., (see Table 2.3) are water soluble. Considering the flame retardant additives in the resins, most

congeners in this broad class are reported as not being water soluble (D'Silva, 2004). However, tetrabromobisphenol-A (TBBPA), which is a principal epoxy resin used in PCBs, is reported to show low water solubility (Chemtura, 2005). This makes the analysis more interesting, and this is the basis for investigations detailed in Section 4.5.1.

The froth stability tests with the pulp of the sample gave a dynamic froth stability height of 5 cm, whilst the filtrate of the pulp of the same solid concentration gave no stable froth that could be measured. The surface tension measurement of the pulp filtrate also gave averages around 72 dynes/cm – similar to that of deionised water. These two observations tend to indicate that the observed frothing is due to something else, other than a soluble heteropolar organic compound in the sample. This is further substantiated by the fact that the actual solubility of the suspect compound (TTBPA) is 0.148 mg/l (Chemtura, 2005); a value about one-hundredth of typical surfactants dosages (Crozier and Klimpel, 1989). Hence it can be safely inferred that the observed frothing is not due to inherent surfactant constituents in the sample.

Another possibility is that this froth resulted from fine particle stabilisation. In this context, it may be necessary to first address some basics of the frothing phenomena. Froth is formed on aerating a solution or a suspension if trapping of air (or gas) bubbles by the liquid film can be achieved. Froth is therefore a dispersed system; it will want to break down spontaneously to lower overall surface and energy (Harris, 1982). This is to say, froth is essentially unstable. Stability of the froth film is, therefore, the major issue in achieving a tangible froth.

In surfactant solutions, overall surface tension is lowered by the surfactant (Section 3.2). This also lowers the free energy difference accompanying surface area reduction. This reduces the spontaneity of breakdown, giving a metastable two-phase froth. In pulps of surfactant solution (as in mineral processing), it is recognised that the stability of the three-phase froth is increased or decreased by solid particles in the pulp – particle size, concentration, shape and degree of hydrophobicity of the solid particles being the interacting factors (Klassen and Mokrousov, 1963; Harris, 1982, Feng and Aldrich, 1999, Pease *et al.*, 2005). With particles of low hydrophobicity, froth stabilisation occurs when a closed packed monolayer of particles is formed in the froth film (Harris, 1982). In this case, the particles attached to the interfaces cannot be

forced out of the film and the two interfaces are kept apart. Flocculation of particles also prevents coalescence of bubbles in the froth (Harris, 1982). This sort of reinforces the film wall.

The other extreme that also exists is stability of froth solely by fine particles in surfactant free pulps. Molecular solutions of compounds such as diacetone alcohol and ethyl acetal (compounds that do not alter solutions surface tension) have been shown to produce adequate froth with fine coal (hydrophobic) particles (Lekki and Laskowski, 1975). Three phase froth has also been generated by aerating a suspension of clean nanosized hydrophilic silica particles in distilled water (Bindal *et al*., 2002). It was submitted that the foaminess observed was directly proportional to particle concentration, inversely proportional to particle size, and the self organization of the colloidal particles into a layered structure between gas bubbles provided a barrier against coalescence, thereby stabilising the foam lamella (Bindal *et al*., 2002).

This brief about froth phenomena is provided to submit that, hydrophilic and hydrophobic particles have been observed to stabilise froth; appropriate particle size is what matters. In a two-phase froth system, lowering of surface tension is a prerequisite, while this is not compulsory to achieve a tangible three phase froth – fine particle stabilisation will suffice. From this standpoint, it is easy to see the possibility of the observed froth resulting from fine particle stabilisation. The sample contains about 65 % passing 38 µm. It was pointed out that the bulk of the finer constituents will be the brittle glass fiber and thermoset (epoxy resin) constituents (see Section 5.2). A close-packed layer of fine hydrophobic particles enveloping gas bubbles in the froth lamella is the major mechanism that can be inferred for stabilisation of the froth. Such stable bubbles floating around at the pulp froth interface are easily seen from the side of the cell. The thick bubble interstices seen in the froth (as in Figure 6.3) also suggest flocculation of particles, thereby reinforcing the bubble walls.

Considering the high mass pull observed (above 50% in most cases, see Figure 6.4), it is also possible to expect that total froth may not result from true flotation due to natural hydrophobicity of some particles alone. Other effects, such as entrainment and entrapment occur in flotation (George *et al*., 2004), and can be expected under such high mass pulls. Fine particles can easily entrain with water, even if not hydrophobic. Strands of copper particles from the PCB traces could also be found in the float fraction, while glass fibers abounds (See Appendix 2).

Entrapment within bubble-particle agglomerates under bulk upward mass transfer will be enhanced by the elongated morphology of such fibrous copper trace and glass particles. For the glass fibers, it will be recalled that in PCB production, the fibers were impregnated with the resin until it sets in place on the fiber. Strong adhesion between the reinforcement and the matrix is a quality requirement in composites. Hence, flotation due to air bubble attachment to the resin impregnated pseudo-hydrophobic surface can be another strong reason for the glass fibers transport to the froth. The various kinetic regimes will be expected to promote the true flotation and other effects differently. This can reflect in how well the responses under each regime fit the first order kinetics.

6.3.2 Kinetic Response

Figure 6.4 shows the cumulative mass pull with time under varying kinetic regimes. The error bars were plotted as the standard error of the mean of the duplicate values for each data point on the plot. The markers tend to eclipse the bars for some points, the standard errors being very small. Data details for the figure and the error analysis are provided in Appendix 2. The E11A condition (see Table 4.1) shows that at the 18 wt. % solid concentration, the proportion of froth-phase bound particles in the cell appeared to be too high that mass pull did not stabilise with time - even after 30 minutes. Driving the rate higher with higher hydrodynamics will simply worsen entrainment and compromise selectivity. The high proportion of the glass fiber particles and its tendency to increase viscosity due to the elongated morphology will also aid this. The lower solid concentration was therefore used in subsequent experiments.

With increasing combinations of the kinetic parameters, the mass pull rate can be seen to increase until the mass recovery curves show definite asymptotes at the experimental conditions of E21C, E22B and E22C. As projected (in Section 6.2), it is notable that this prevailing kinetic condition, which suffice to keep the particles in suspension, corresponds to impeller energy and aeration rate much lower than what is found in conventional flotation of ores that also liberate in this fines size range. This can be connected to the much lower aggregate density of this sample.

As expected, the observed mass pull rate varied over time for the different regimes. Considering the regimes with fully defined responses under the time interval (with asymptotes in Figure 6.4),

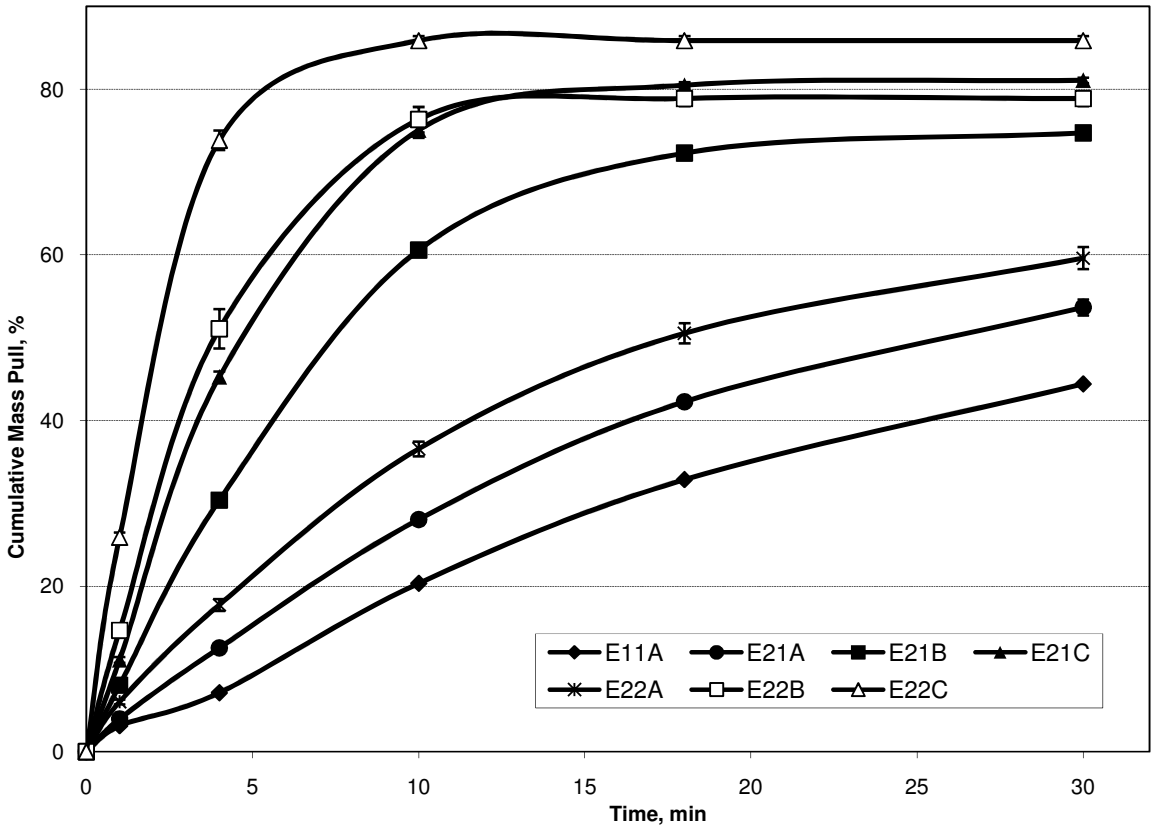

Figure 6.4: Cumulative mass pull with time under natural hydrophobic response and varying kinetic parameters.

mass pull under E21C became very faint in the last 18 to 30 minutes; under E22B, mass pull stopped at around 12 minutes of flotation. For E22C, mass pull ended under 10 minutes (Appendix A2: Table A2.4). The extent of fit of the responses to the classical first order model (Equation 4.1) is shown in Figure 6.5. Detail of the fitting data is shown in Table A2.6. E22B clearly shows overall higher kinetics compared to E21C, whereas the cumulative plots for the two regimes give competing performances in Figure 6.4. The higher correlation coefficient shows E21C conforms more to the first order trend in Figure 6.4. Although the responses under E22B and E22C regimes ended earlier due to the higher prevailing kinetics, so that the fits are fully described with fewer points, yet the responses fit well while they last. In general, all the conditions gave good correlation, and this indicates that the observed responses conform to describable froth flotation phenomena. However, the reverse enrichment of the desired metallic values into the sinks will give surer basis for assessing the performance of the scheme.

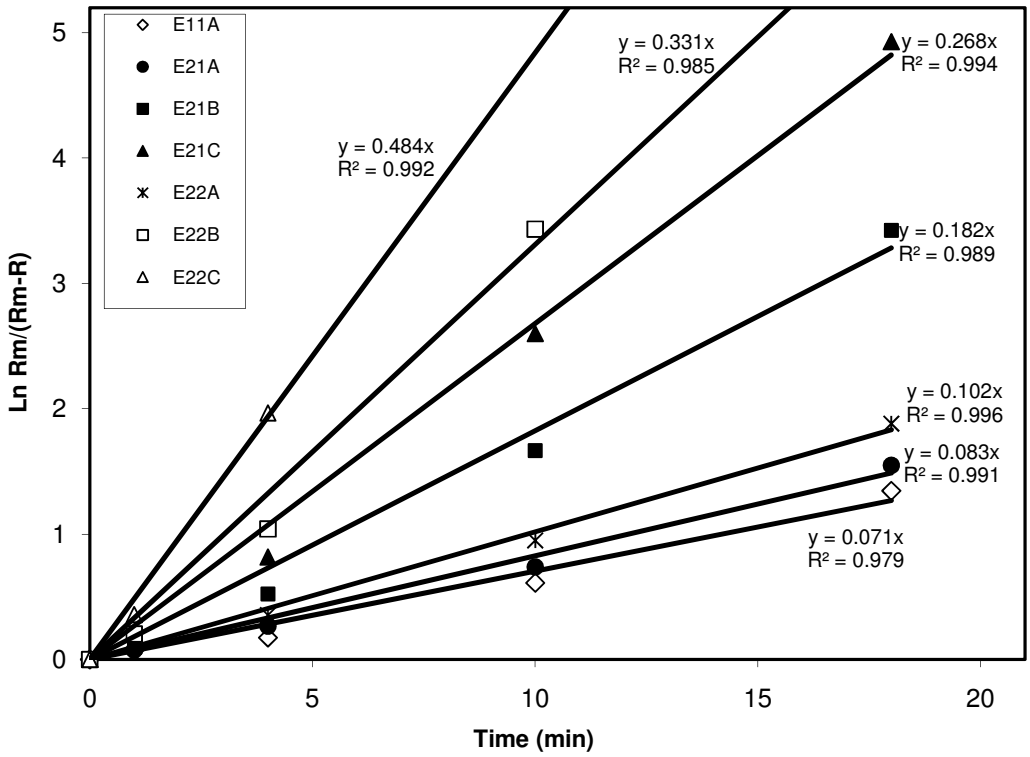

Figure 6.5: First order fitting of PCB comminution fines NHR under various kinetic regimes

6.3.3 Sink Enrichment: Digested Total Metallic Content

Figure 6.6 summarises the sinks' enrichment based on the fractional digestion data, as described in Section 4.5. Relevant data and computation details for the figure are shown in Appendix A2. The general trend shows assay-recovery tradeoff typical of beneficiation operations. The low enrichment levels (assays) indicated for E11A and E21A confirms the inadequate pulp density and kinetics noted for these conditions. The highest recovery in E11A merely indicates that the bulk of the feed (concentrate mass being 55% of feed) still remains in the sink; 100 % recovery to sink can as well be achieved by carrying out no beneficiation. E22C gave indication of the best metallic assay as being 43 %, but with the worst compromise on recovery. E21C and E22B with close performances based on kinetic assessment, appear to give the best combinations of assay and recovery, with 42 % and 38 % assays and recoveries of 39% and 41% respectively.

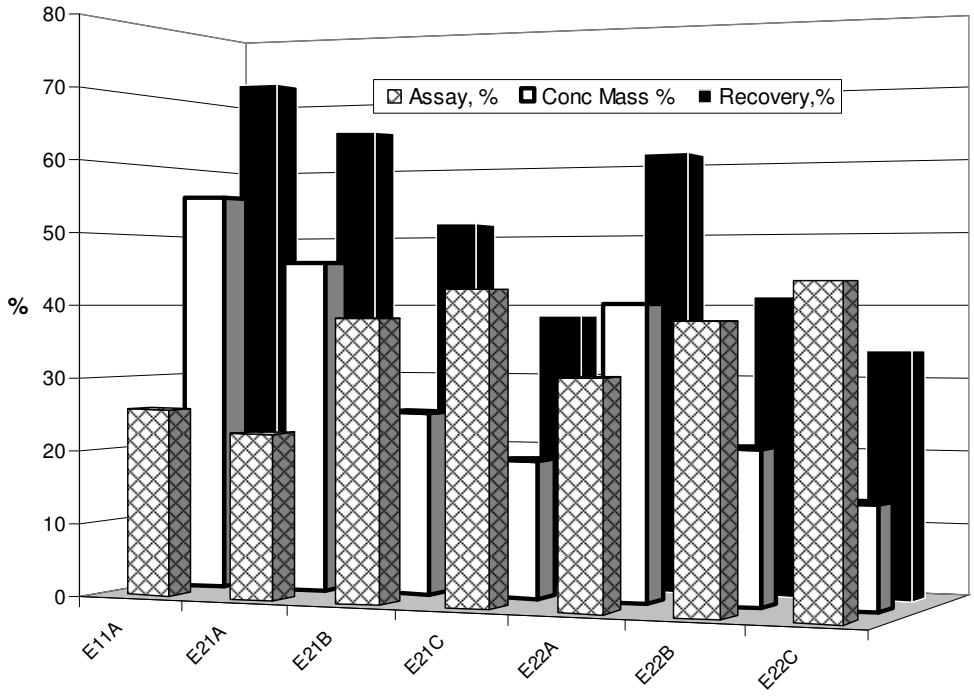

Figure 6.6: Indications of enrichment of metallic values into the sink fraction. *(Metallic assay inferred from total fraction digested. Concentrate mass percent is the proportion of final sink to feed and recovery of metallic values to sink based on the indicated assay value)*

As these responses are based on the natural hydrophobic response, with no collector or frother and no treatment to alter hydrophobicity, the responses must be explained from the kinetic parameters variation. From the flotation cell operation, higher impeller speeds, at constant aeration, produce finer bubbles. The figures in Appendix A2.5 show frozen frames that give visual indications of sizes at the various kinetic regimes. Finer bubbles at constant aeration imply higher bubble surface area, lower buoyancy and increased bubble residence time. Increased turbulent dissipation energy is also a direct effect of higher impeller speed. All these factors increase the efficiency of particle bubble collision (Duan *et al*., 2003; Pyke *et al*., 2003). With favourable surface conditions for attachment, higher collision efficiency in turn gives higher collection efficiency.

Taken to the extreme, this condition (increasing impeller speed and consequently lower bubble sizes) can also increase turbulent carry-over and entrainment at the expense of the reverse recovery. Froth interstices, which are conduits for entrainment, increase. Resultant upward momentum also increases resistance to sinking for otherwise sink-fraction particles. Hence,

higher mass pull (lower sink concentrate mass) was observed from increasing impeller speeds, as can be seen in Figures 6.4 and 6.6, when comparing E22A, E22B and E22C, or E21A, E21B and E21C. It follows that a lower concentrate mass resulted in a lower reverse recovery; this implies target value loss to the high mass pull. Conversely, assay increased with a lower concentrate mass and a lower reverse recovery as more froth phase particle could rise at the higher mass pull, leaving a smaller but richer sink.

The performance across the category can also be resolved on this basis. Studying the response under E21C and E22B regimes, the result reflects the interplay of superficial gas velocity (J_g, cm/s), the superficial surface area flux (S_b, s^{-1}) of bubbles and the actual bubble sizes (d_b, cm) on the observed recovery and rate. S_b is a function of J_g, which is a function of aeration rate (Q), but S_b is also dependent on d_b (Vera *et al.*, 1999; Schwarz and Alexander, 2006):

$$S_b = {}^{6J_g}/_{d_b} \quad . \quad . \quad . \quad . \quad . \quad . \quad . \quad . \quad . \quad 6.1$$

while,

$$J_g = {}^{Q}/_{A} \quad . \quad . \quad . \quad . \quad . \quad . \quad . \quad . \quad . \quad 6.2$$

where A is the cross-section area of the cell.

It follows that increasing Q increases J_g and vice versa. However, if such operation alters d_b simultaneously, S_b will not change proportionately. Under the regimes in focus, in moving from E21C to E22B, bubble size was increased both by increasing Q and lowering the impeller speed. Table 6.1 gives ratios of these parameters under these regimes at the constant cell cross-sectional area and based on the estimates of d_b in Appendix A2.6.

Table 6.1: Ratio of some kinetic parameters under E21C and E22B regimes

Parameters	Ratio of parameters under regimes	
	E21C Regime	E22B Regime
Aeration rate, Q	1	2
Superficial gas velocity, J	1	2
Bubble diameter, d_b	1	2.5
Superficial surface area flux, S_b	1.25	1

Connecting this to what was observed, the higher buoyancy of the larger bubbles under E22B, and the larger flow rate reflected in the higher rate constant. But with a lower residence time of the much larger bubbles, particle-bubble collision probability became so low after substantial mass was pulled that mass pull ended around 12 minutes (see Figure 6.4). Under E21C, on the other hand, the higher residence time of the finer bubbles (at higher impeller speed), with the high surface area of bubbles flowing through, maintained collision efficiency such that mass pull persisted after 18 minutes. The E21C regime thus compensated for half the air flow rate and achieved overall higher mass pull over time compared to E22B. However, this extra pull turned out to be a disadvantage based on the elemental analysis of sink enrichment with time.

6.3.4 Sink Enrichment: Elemental Analysis

Table 6.2 shows reconstituted feed assays of selected elements from the float and sink fractions from the batch samples for each investigation, averaged with assay of a direct feed sample. This gives a total of 14 assays averaged for each element. The relative standard deviation for each element in the table gives an indication of how the assays compare in all the batch samples. It shows that the batch samples were generally representative of the bulk, most of the relative standard deviations being under 5%.

Obvious extremes are Pt and Ag, showing that the reasons may be more than sampling variation. Pt reflects the analytical limitation of ICPOES for trace quantities. Ideally, ICP MS is supposed to complement ICP OES with respect to the trace quantities. The analysis at this stage of the investigation being voluminous, with 135 leach solutions, only ICPOES was used because of cost constraints. Silver (Ag) showed peculiar analytical challenges possibly due to light sensitivity of the element and the effects of this on its emission spectra. Ag would have been

better analysed individually using AAS (atomic absorption spectroscopy) rather than multi-element analysis. Again, the constraint is the same. However, to account for any possible variation in feed assays, reconstituted assay for each batch flotation feed was used in all the recovery analyses.

Table 6.2: Reconstituted feed assay of select elements

Element	Average Assay (ppm)	Relative Std. Dev. (%)
Ag	662	19.99
Al	34 864	0.81
Au	202	5.68
Ca	70 078	2.92
Cu	36 783	2.63
Fe	27 656	1.20
Mg	2 001	1.88
Ni	2 195	2.85
Pb	26 007	1.19
Pd	162	1.64
Pt	2	100.8
Si	280	12.79
Sn	36 855	2.25
Ti	2 748	2.38
V	33	2.14
Zn	5 975	3.77

Table 6.3 summarises the recoveries and enrichment ratios of specific elements for all the sinks, while separate plots of the enrichment ratio (ER) versus reverse recovery in the sinks over time for some selected elements under the different kinetics are shown in Figures 6.7 to 6.13. Analytical data and computation details for the figures are presented in Appendix 3. Enrichment ratio (ratio of concentrate to feed assays) has been used to give a uniform basis for comparison as the assays range from ppm to percentage levels for the different elements. In addition, with the assay scale, a response can lie above another, even at t = 0 (that is, before any enrichment), due to feed sample assay variations in such heterogeneous stock. Feed sample assays for gold, for instance, in this analysis ranged, from 190 to 219 ppm, while the range for Pd was 160 – 165 ppm.

Considering the response of gold, the best recovery of 79% was obtained at the lowest ER of 1.72 under E12A conditions. The best ER of 3.65 was achieved with a recovery of 51% under E22C experimental condition (Table 6.3). A combination of 64% recovery and 3.05 ER was obtained under the E22B condition. This can be considered optimum relative to E21C, which gave a recovery of 58% at almost the same ER of 3.08. This is an actual assay of 626 ppm at 58% recovery in the case of E21C, with an equivalent concentration of 622 ppm at 64% recovery for E22B. Trading off such little enrichment for a 6 % higher recovery is a good economic judgment for precious metals. The picture is made clear in Figure 6.7 which shows the E22B plot lying well ahead (higher recovery) that of E21C.

For palladium, the E22B plot (see Figure 6.8) also lies clearly ahead and above (higher enrichment) that of E21C showing a notably better performance, with the final assay being 456 ppm at 58 % recovery under E22B. Ni and Zn are other elements for which E22B can be taken as giving the best performance (see Table 6.3), with actual assays of 5562 ppm and 1.43%, respectively.

Table 6.3: Recoveries (Rec) to and Enrichment Ratios (ER) in the sinks for specific elements

Elements	E21A		E21B		E21C		E22A		E22B		E22C	
	Rec, %	ER	Rec, %	ER	Rec, %	ER	Rec, %	ER	Rec, %	ER	Rec, %	ER
Ag	42	0.93	24	0.80	19	1.04	32	0.79	18	0.87	17	1.18
Al	46	0.99	22	0.74	16	0.83	39	0.96	18	0.88	12	0.88
Au	79	1.72	68	2.52	58	3.08	77	1.90	64	3.05	51	3.65
Ca	42	0.92	19	0.63	12	0.66	35	0.87	15	0.72	10	0.67
Cu	66	1.44	47	1.70	38	2.04	61	1.53	41	1.93	31	2.21
Fe	61	1.35	42	1.51	33	1.76	56	1.38	35	1.65	27	1.93
Mg	45	0.98	23	0.79	17	0.90	39	0.96	20	0.93	14	1.02
Ni	76	1.65	60	2.21	50	2.66	72	1.78	54	2.56	42	2.97
Pb	74	1.60	55	2.02	45	2.37	67	1.68	46	2.20	34	2.40
Pd	80	1.74	64	2.37	52	2.74	77	1.91	58	2.76	46	3.23
Si	37	0.82	27	0.93	30	1.57	45	1.11	31	1.47	32	2.23
Sn	70	1.53	51	1.84	40	2.12	64	1.58	42	1.98	30	2.09
Ti	81	1.77	72	2.70	66	3.52	79	1.96	67	3.21	61	4.31
Zn	73	1.58	56	2.05	47	2.50	68	1.70	51	2.44	43	3.05

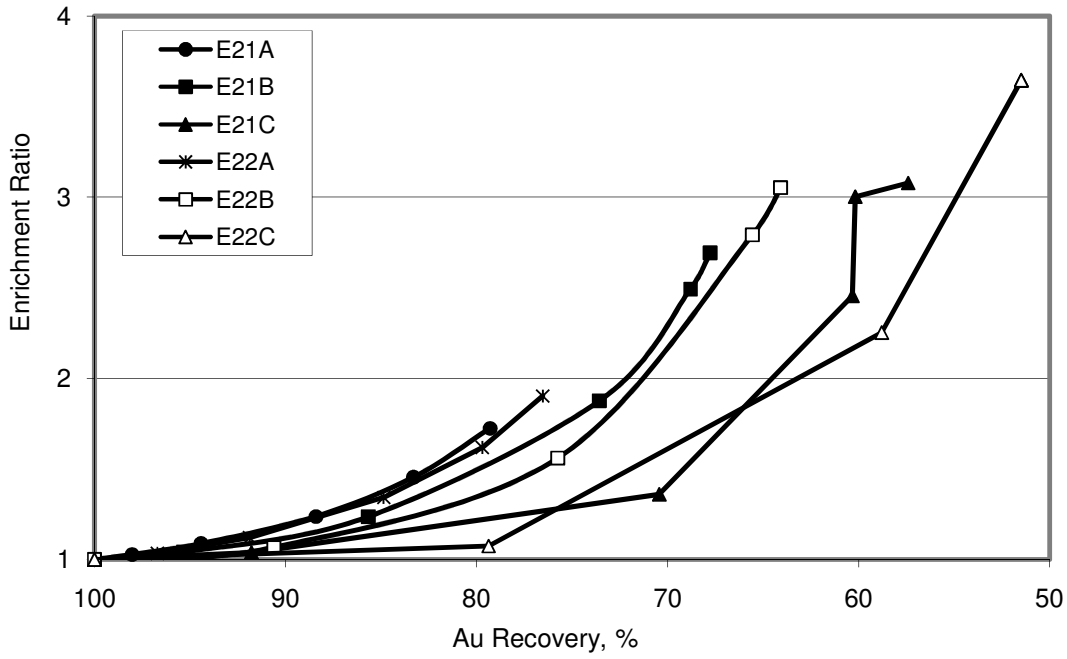

Figure 6.7: Enrichment ratio vs. recovery of Au to sinks under varying kinetic regimes.

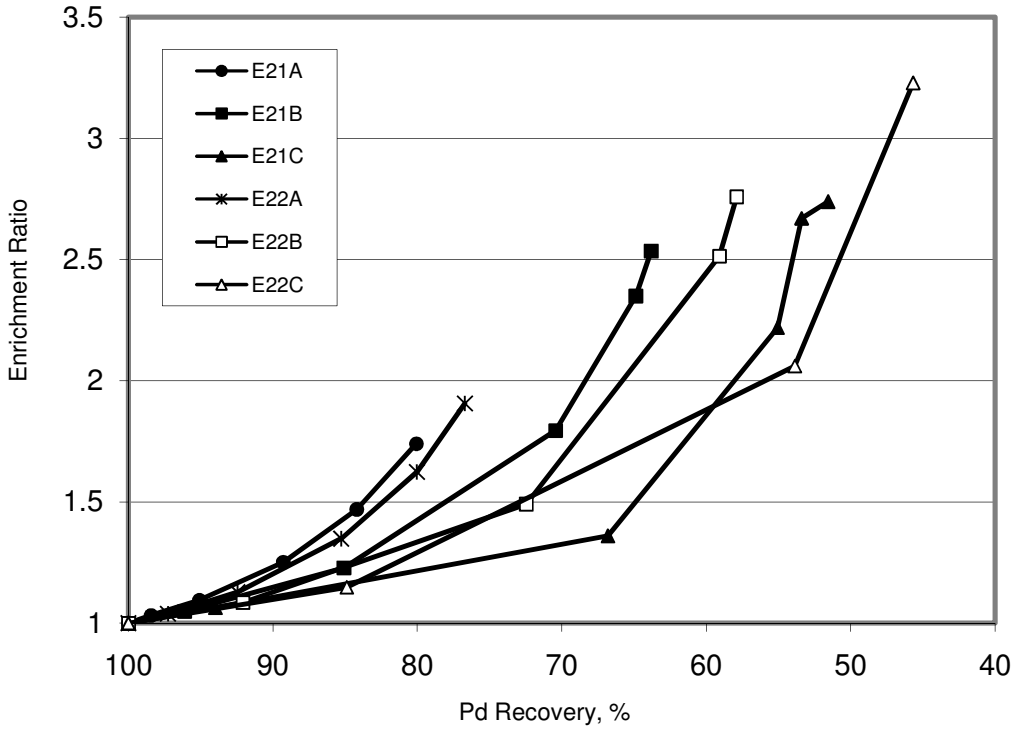

Figure 6.8: Enrichment ratio vs. recovery of Pd to sinks under varying kinetic regimes.

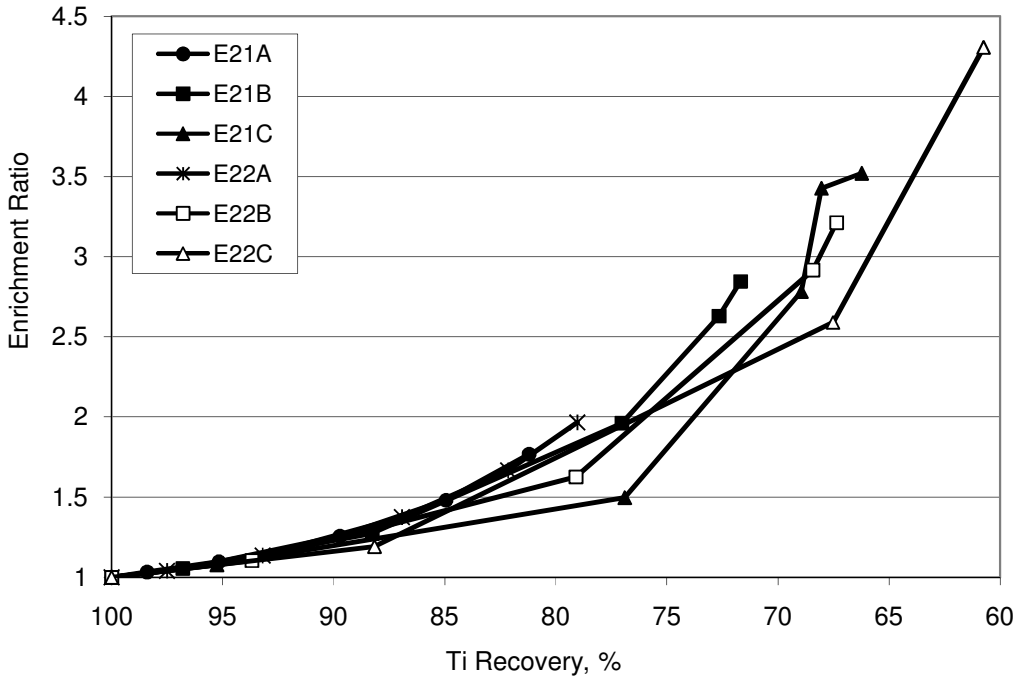

Figure 6.9: Enrichment ratio vs. recovery of Ti to sinks under varying kinetic regimes.

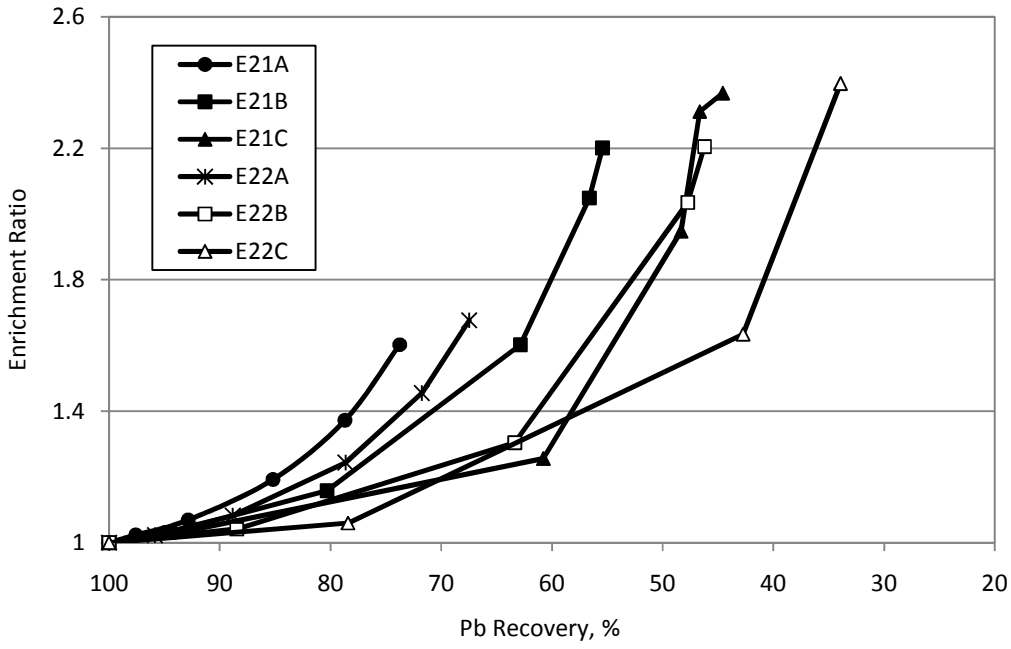

Figure 6.10: Enrichment ratio vs. recovery of Pb to sinks under varying kinetic regimes.

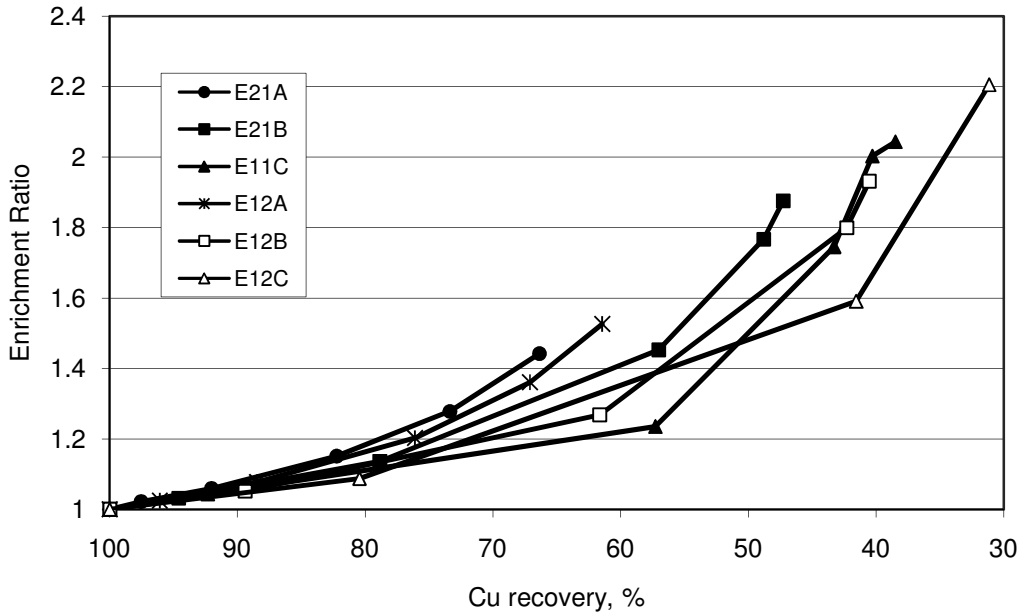

Figure 6.11: Enrichment ratio vs. recovery of Cu to sinks under varying kinetic regimes.

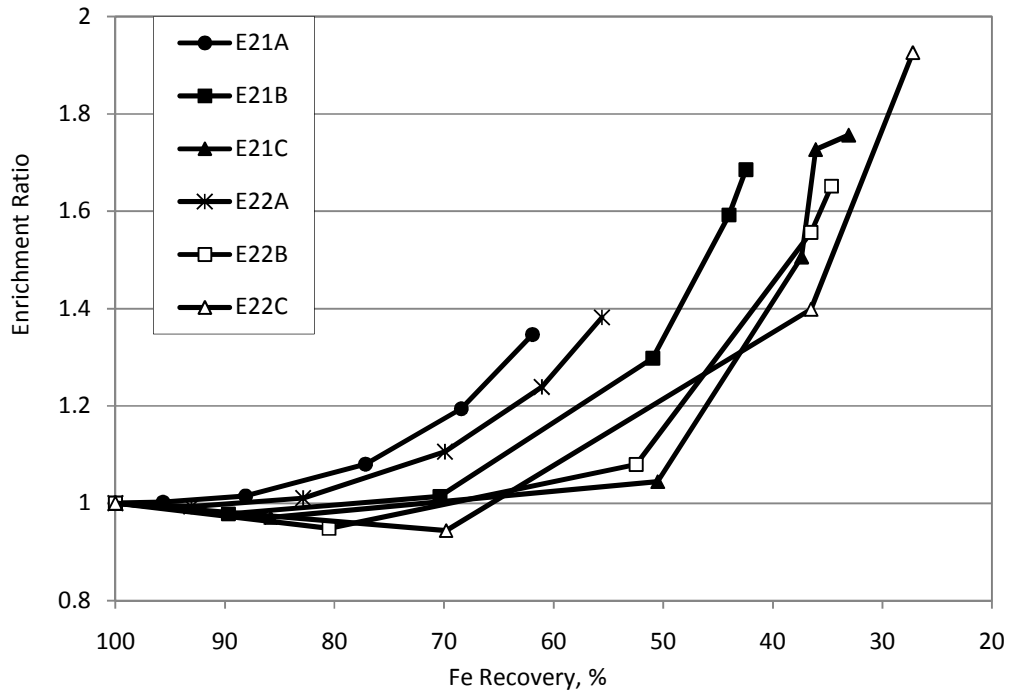

Figure 6.12: Enrichment ratio vs. recovery of Fe to sinks under varying kinetic regimes.

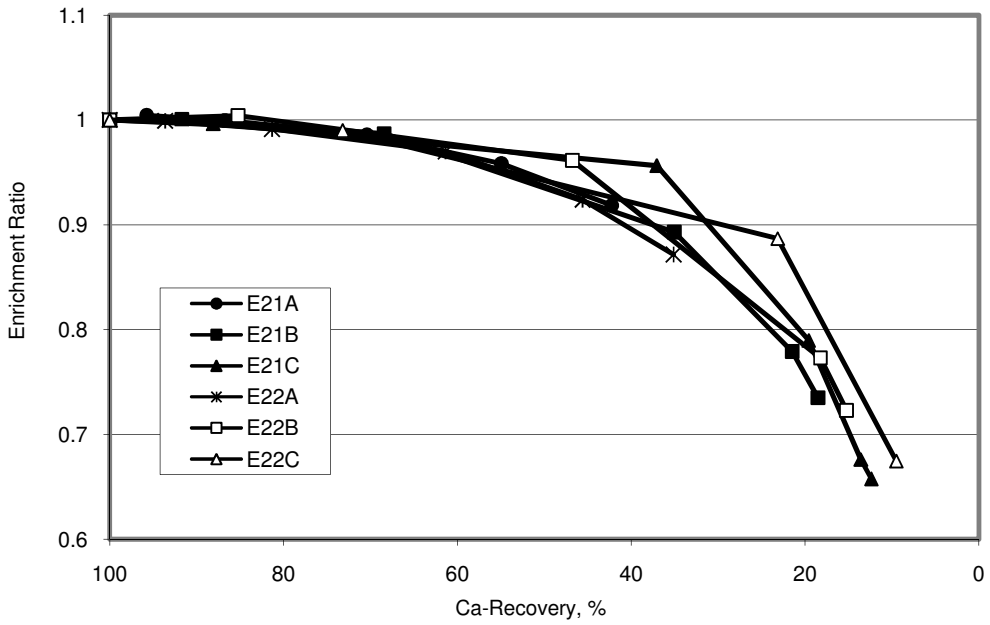

Figure 6.13: Enrichment ratio vs. recovery of Ca to sinks under varying kinetic regimes.

For Ti and Pb, a careful observation of the responses in Figures 6.9 and 6.10 shows that E21C gave a better performance than E22B. Before 18 minutes of flotation, mass pull under E22B conditions stopped (Figure 6.4), while under E12C condition, little mass pull still continued until the 30th minute of flotation. In this last interval, a disproportionate drop in recovery versus ER in all the E21C plots in Figures 6.7 to 6.12 can be observed. Plots of Sn and Zn (not shown) also show the same trend. Comparing the two kinetic regimes at the end of 18 minutes, E21C gave better enrichment ratios and better or almost equal recoveries when compared with E22B. This implies that E21C operating parameters should have run for 18 minutes, as for E22B, in order to result in better ER and recovery for these elements.

The response for Fe (Figure 6.12) also shows best performance under E21C, though with high compromise on recovery, dropping down to 37 % at 18 minutes. With E22B and E22C condition, a worse performance of negative enrichment could even be observed at some stages in the pulp. This negative enrichment is more pronounced with Ag, Mg and Al (Table 6.3), showing that these elements prefer the froth phase. Recoveries dropped below 20 % at ER of 0.9 under E21C for Mg, for instance. Ca is of special interest due to its significant proportion ~7 % by mass in the feed (Table 6.2). Consistent reduction in Ca assays in the sink fractions over time

(negative ER) for all the kinetic regimes can be seen in Figure 6.13, giving less than 15 % residual recovery in the sink for E21C. Platinum assays were too low – a few ppm – for purposes of reliable analytical figures (see relative standard deviation of Pt assay in Table 6.2).

To explain these responses, it is expected that metallic particles reports to the sink. Metallic particles will have a high surface energy, be hydrophilic (Gupta and Yan, 2006) and therefore prefer the sink. Density advantage is also expected here to enhance the separation between denser hydrophilic metallic particles and lighter hydrophobic plastic particles. The questions then will be: Why is recovery to sink not 100% for such metals, and why do some metallic elements preferentially report to the froth?

It is necessary to appreciate that the elements are contained in particles occurring as some end-use alloy or compounds. These particles are present in diverse shapes, and can still be part of a composite particle. Considering the fact that composite particles still exist in this sample (see Section 5.2), the response of elements occurring in such particles would not be expected to be perfect. Comminution of ductile metallic materials generally produces particles with random shapes (Section 5.2), including flattened pieces that will have a tendency to float around in the pulp, particularly in this size range. Gold flakes float for this reason in conventional minerals flotation circuits (Allan and Woodcock, 2001).

The split of Cu to the float and sink stream is another example that can be readily attributed to shape influence. Copper particles from the PCB traces remain in elongated forms (Figure A2.5) that can be easily carried over into the froth by rising masses and bubbles. Hence, short strands of the PCB copper trace were found in the float, as noted previously (see Section 6.3.1). On the other hand, those from copper nuts, edges, etc., which could have chipped into a more cubical particle, can resist the upward current and report better to the sinks.

For metals preferring the froth phase, probable reasons could also be the size and shape in which particles occur. For instance, Al, Ca, Mg from the oxides (see Table 2.4) will occur more in the finer sizes from comminution of the ceramics. Separate elemental analysis of −38 µm and −75+38 µm size fractions of the fines sample (see Table A2.11 and Appendix 2) show all the metals have higher assays in the coarser fraction (allowing for a minimum 10% difference for significance), except Al and Ca. The brittle ceramics containing Al and Ca would have

undergone more selective pulverization relative to the ductile metallic alloys. The much finer particles will be entrained with water at the prevailing kinetic condition more easily than the relatively larger particles. It is expected that favourable kinetics will differ among particles in the whole -75 µm size range (Pease *et al*., 2005). However, fine Al bearing particles can also occur as flattened chips from the ductile alloy. Chances are that the flat or foil mini-chips, coupled with low density of aluminum, can be carried under bulk upward mass transfer of the glass fibers. The same shape factor can be expected to influence Mg, being even lighter than Al.

From the foregoing discussions, it follows that the interacting mechanisms that could be responsible for the responses observed include: natural hydrophobic response to float and hydrophilic preference for the sink; presence of hydrophobic material on an otherwise hydrophilic surface; particle morphology (shape) enhanced carryover under bulk upward mass transfer; and fine particle entrainment in water to froth. The kinetic regimes investigated were seen to promote these factors differently as the responses vary with kinetic conditions. To one extreme of kinetics, recovery can be extremely compromised, and to the other, enrichment.

The actual range of values at which the kinetic parameters will give the most favorable regime to optimize the performance will of course vary to some extent among cells (O'Connor *et al*., 1987). In the present observation, the favorable range is 400 rpm impeller speed with 1000 ml/min aeration to 500 rpm with 500 ml/min aeration (the range for E21C and E22B regimes). This gives an indication of the low energy (turbulence) requirement of this sample relative to conventional mineral flotation. The analysis also shows that the interactions of the various factors favor enrichment and recovery of Au and Pd to the sink. The response from these precious metals, which are the economic drivers for PCB resource recovery, shows the scheme can indeed be prescribed for PCB comminution fines beneficiation.

6.3.5 Improving the Performance of the Natural Hydrophobic Response Scheme

With the recovery values across the elements from the NHR scheme, performance improvement is conceivable. The observed float fraction being so high, it was projected that the kinetics of the operation should be slowed down to reduce mass pull rate. The intention was that lower mass pull rate would allow true flotation to be more pronounced, while entrainment and entrapment would be minimized. With about 65% passing 38 µm in this sample, and recognising that the

same kinetic regime cannot favour all the particles in the -75 µm range (Pease *et al.*, 2005), a narrower size distribution was also probable for better performance. Investigations in this regard are detailed in Section 4.5.2.

The impeller modification indeed gave glaringly smaller bubble sizes at the 300 rpm impeller speed, compared to what was obtained before modification (see figures in Section A2.5, Appendix 2). Coupled with the sample size of 150 g, the turbulence in the cell is much more moderate. After 18 minutes, mass pull rate at 300 rpm was observed to become very slow in the initial trial runs, and the impeller speed had to be increased to 350 rpm to increase particle bubble collision and sustain the pull. Investigations with this kinetic regime was designated XNHR. Table 6.4 shows the averaged cumulative mass pull for triplicate experiments. The raw data is contained Section A2.7, Appendix 2. Compared to the initial responses, shown in Figure 6.4, it can be observed that the prevailing kinetics after the impeller modification gave generally lower cumulative mass pulls. The response was closest to what was obtained under E21A conditions (see Table 6.3). In these two regimes (E21A and XNHR), the effect of smaller bubble size on the kinetics compensated for lower solid concentration (collision frequency), such that the cumulative mass pull in the same time interval was comparable.

Table 6.4: Cumulative mass pull after impeller modification

Time (minutes)	Cum Mass Pull (%)	Standard Deviation
18	41.2	1.8
30	52.5	1.2
48	57.7	0.4

In the final analysis, the intention was to achieve an: increase in recovery of metallic values to the sink without compromising the enrichment level obtained; increase in enrichment while maintaining recovery levels; or increase in both. Table 6.5 shows the enrichment ratio and recovery levels in the prevailing kinetics compared to what was obtained in some of the previous conditions. Based on this elemental analysis, the performance is again almost the same as in the E21A regime and a remarkable improvement may not be inferred. This could show that equivalent cumulative mass pull over a given time is effectively an indication of similar kinetic regimes. A more definite difference in performance can therefore be expected if equivalent mass pull is obtained over a different time interval. On this basis, the performance after 48 minutes can

be compared to what was obtained in E22A, which gave a comparable cumulative mass pull of 59% after 30 minutes. Still a drastic improvement may not be inferred, because the little increase in recovery appeared to be due to the sink fraction being a bit larger and ER dropped off a little for the increase.

Table 6.5: Comparison of reverse metallic recovery (Rec) versus enrichment ratio (ER) before and after impeller modification

	XNHR - 18 mins		XNHR - 30 mins		XNHR - 48 mins		E21A - 30 min		E22A - 30 min	
Element	**Rec, %**	**ER**	**Rec, %**	**ER**	**Rec, %**	**ER**	**Rec, %**	**ER**	**Rec, %**	**ER**
Ag	59.1	1.01	46.1	0.98	40.8	0.97	41.9	0.93	31.76	0.79
Al	57.6	0.98	45.3	0.96	40.1	0.95	45.7	0.99	38.81	0.96
Au	85.4	1.46	80.2	1.70	78.2	1.86	79.3	1.72	76.53	1.90
Ca	56.1	0.96	43.0	0.91	37.4	0.89	42.3	0.92	35.11	0.87
Cr	63.5	1.08	53.3	1.13	48.3	1.15	-	-	-	-
Cu	74.8	1.27	68.1	1.44	64.7	1.54	66.4	1.44	61.42	1.53
Fe	65.2	1.11	55.2	1.17	51.6	1.23	61.9	1.35	55.59	1.38
Mg	59.5	1.01	47.3	1.00	41.4	0.99	44.9	0.98	38.78	0.96
Ni	80.1	1.36	73.9	1.57	71.2	1.70	76.1	1.65	71.57	1.78
Pb	77.2	1.32	69.9	1.48	67.0	1.60	73.7	1.60	67.47	1.68
Pt	82.5	1.41	77.4	1.64	75.1	1.79	-	-	-	-
Pd	84.0	1.43	78.3	1.66	76.0	1.81	80.1	1.74	76.71	1.91
Sn	75.0	1.28	67.0	1.42	64.0	1.52	70.4	1.53	63.76	1.58
Ti	86.7	1.48	82.2	1.74	80.0	1.90	81.2	1.77	79.02	1.96
V	62.2	1.06	51.3	1.09	46.5	1.11	53.6	1.17	46.61	1.16
Zn	81.1	1.38	75.5	1.60	72.6	1.73	72.9	1.58	68.44	1.70

The summary observation, therefore, is that if the kinetics is slowed down too much, in an attempt to pull slowly over time, particle bubble collision gets too much compromised and even the natural hydrophobic particles recover poorly. This is what was observed when the impeller speed had to be increased to 350 rpm under XNHR, otherwise a bulky sink would be obtained with minimal enrichment. If the kinetics is also to the extreme, the froth phase particle can be pulled more effectively, leaving a cleaner sink but grossly compromising the reverse recovery. At the reduced kinetics, when comparing achieved reverse recovery and enrichment, the idea of minimizing turbulence and a slower mass pull rate does not appear to improve selectivity. The bulk flotation behavior of the sample basically remains the same: the higher the mass pull, the

lower the reverse recovery and the higher the reverse enrichment. In other words, at the lower kinetics, reverse recovery loss to float still occurs in proportion to the mass pull. The investigation over narrower PSDs provides useful insight to reconcile this.

Figure 6.14 shows cumulative pulls over 30 minutes at narrower and varying sample PSDs. Comparing the mass pulls, the −38 µm fraction gave the highest mass pull, while the −106 + 75 µm fraction gave the least. At the same sample mass of 150 g, the actual number of particles in the samples for each of the size classes certainly differed widely. This translates into a major difference in the kinetics of particle bubble mass removal, which reflected in clear differences in the cumulative mass pulls. This again shows that cumulative mass pull over a given time is a major indicator for effectively different kinetic regimes. Also, the responses further support the submission on fine particle stabilisation of the NHR froth, as the coarsest size fraction pulled least mass. With less stable froth, bubbles lose part of their particle load back to the pulp.

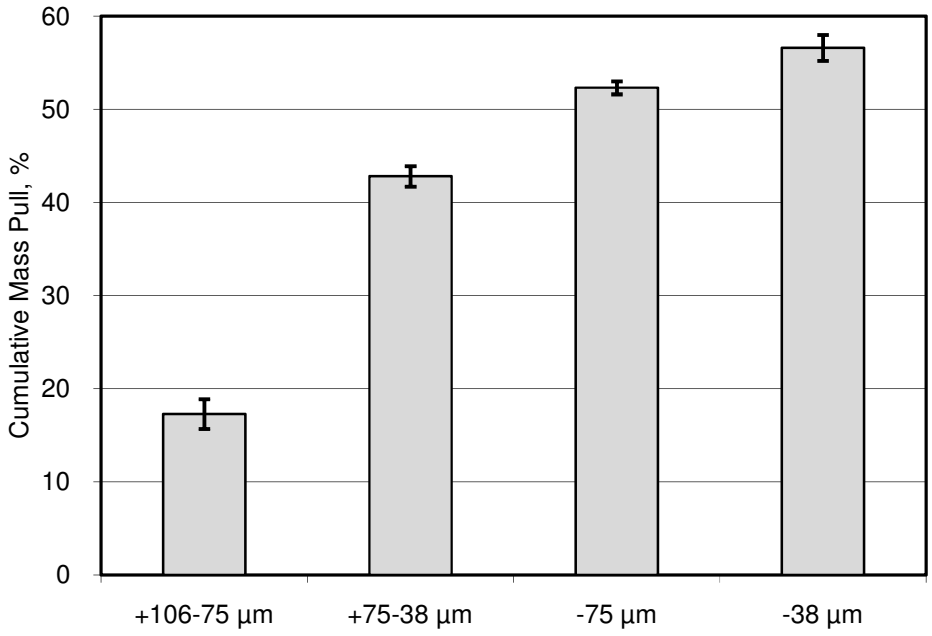

Figure 6.14: Cumulative mass pulls after 30 minutes for varying sample PSDs

Table 6.6 shows the recovery and enrichment ratios obtained from the fraction assays, while Figure 6.15 shows a comparison of the performance for specific elements – Au, Pd and Cu –

over the different size ranges. Comparing − 75+38 µm and −38 µm fractions, the coarser size clearly shows better recoveries and enrichment ratios. For Au, Pd and Cu for instance (see Figure 6.15), recoveries were 91.2%, 92.8% and 86.3%, with enrichment ratios of 1.6, 1.62 and 1.51 respectively for −75+38 µm. For the same elements, recoveries were 64.9 %, 66.5 %, 62.7 % and enrichment ratios 1.44, 1.48 and 1.39, respectively for −38 µm fraction. The prevailing (XNHR) kinetics obviously favours the coarser fraction. This implies that operating at narrower PSD and favourable kinetics for each size fraction will achieve better performance from the NHR scheme, compared to processing wide PSDs, such as the −75 µm fraction. As can be seen, the recoveries from the −75+38 µm are clearly higher than for the −38 µm fraction, without compromising the enrichment ratios.

Table 6.6: Comparison of reverse recoveries and enrichment ratios for varying sample PSD

Element	Recovery, %				Enrichment Ratio			
	105-75µm	-75 µm	75-38 µm	-38 µm	+106-75µm	-75 µm	75-38 µm	-38 µm
Ag	93.3	46.1	63.0	29.3	1.14	0.98	1.10	0.65
Al	79.8	45.3	47.6	44.7	0.97	0.96	0.83	0.99
Au	97.6	80.2	91.2	64.9	1.19	1.70	1.60	1.44
Ca	75.0	43.0	42.3	43.2	0.91	0.91	0.74	0.96
Cr	93.2	53.3	67.3	50.2	1.14	1.13	1.18	1.12
Cu	97.7	68.1	86.3	62.7	1.19	1.44	1.51	1.39
Fe	95.6	55.2	69.8	54.0	1.17	1.17	1.22	1.20
Mg	80.7	47.3	49.3	45.8	0.98	1.00	0.86	1.02
Ni	98.4	73.9	88.5	68.4	1.20	1.57	1.55	1.52
Pb	98.5	69.9	88.2	61.6	1.20	1.48	1.54	1.37
Pt	98.2	77.4	93.1	68.9	1.20	1.64	1.63	1.53
Pd	99.0	78.3	92.8	66.5	1.21	1.66	1.62	1.48
Sn	98.3	67.0	86.5	60.4	1.20	1.42	1.51	1.34
Ti	98.6	82.2	92.9	78.0	1.20	1.73	1.74	1.63
V	90.3	51.3	58.6	51.2	1.10	1.09	1.03	1.14
Zn	97.8	75.5	89.5	70.0	1.19	1.60	1.57	1.55

This result shows that the higher mass pull at −38 µm fraction compared to the −75+38 µm fraction resulted in a lowering of enrichment. This would either be due to non-selective entrainment of sink values with water at the higher mass pull or to pure entrapment and carry-over under heavier upward mass transfer. The water recoveries observed over the different size classes is shown in Figure 6.16. The figure shows cumulative mass recoveries to froth versus

cumulative water recoveries over 30 minutes of flotation. The result shows that the finer size fractions recovered less water per unit mass pull compared to the other sizes, as the slopes in the figure indicate. This tallies with observation during the experiment, as the froth from the finer fractions was well drained and drier, with a high dynamic froth height; the coarser fraction was more like a muddy scum and wet (see Appendix 2.7). It is notable here that stability of the froth in the finer fraction does not rely on low surface tension liquid film, hence the air bubbles enveloped by fine hydrophobic particles rising to the froth in the finer size fraction can be expected to entrain less water. The froth from the coarse fraction, on the other hand, being less stable, collapses into a mud that does not allow effective drainage of water trapped within it.

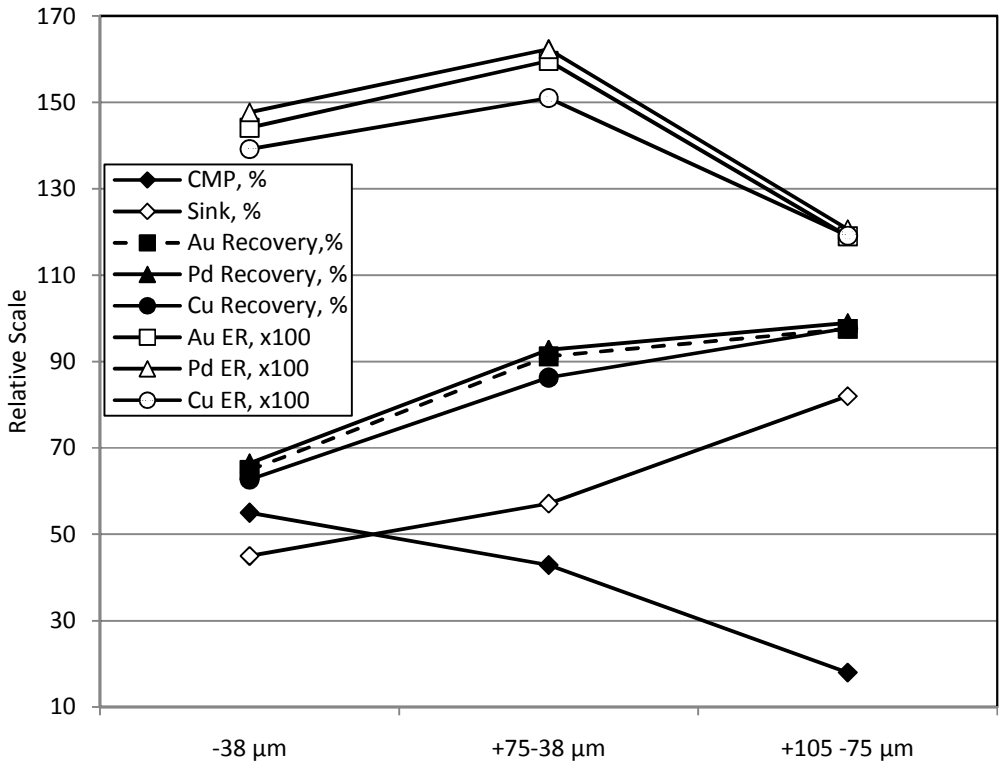

Figure 6.15: Comparison of NHR performance with varying particle size range *The y-axis is a numerical scale to indicate percentages for the cumulative mass pull (CMP) and recovery data, as well as the enrichment ratios (ER) multiplied by a factor of 100 (to accentuate the differences).*

The interpretation that follows from this is that reverse recovery loss due to water entrainment in the finer fraction should be lower, as this fraction recovers less water per unit mass to froth. The higher loss of value to the froth in the finer fraction, which occurs at higher mass pull, should

therefore be due to non-selective transport of sink particles to the froth phase by carry-over under the heavier upward mass transport and entrapment in the froth phase. This effect will be significant in this flotation system where it is the bulk that is responding under natural hydrophobicity and the particles being entrapped constitute a very small proportion.

It will also be noted that the particles rising to the froth also consisted of glass fibers in the bulk. Such particles make the flow more viscous and thus tinier particles are easily dragged along. It follows that the observed bulk NHR response of the sample will be difficult to reverse in favour of the metallic particles that are in a much smaller proportion, hence a recovery versus assay tradeoff occurs readily, as observed when comparing the treatments. The poorest enrichment at the coarsest fraction that recovers the largest amount of water per unit mass pull is understandably due to generally low upgrading, as the bulk remains in the sink and may not be taken as entrainment of the coarse particles with water. The fact that observed recovery at the coarsest fraction is so high (discussed below) shows that the relatively high water pull per unit mass was not entraining values.

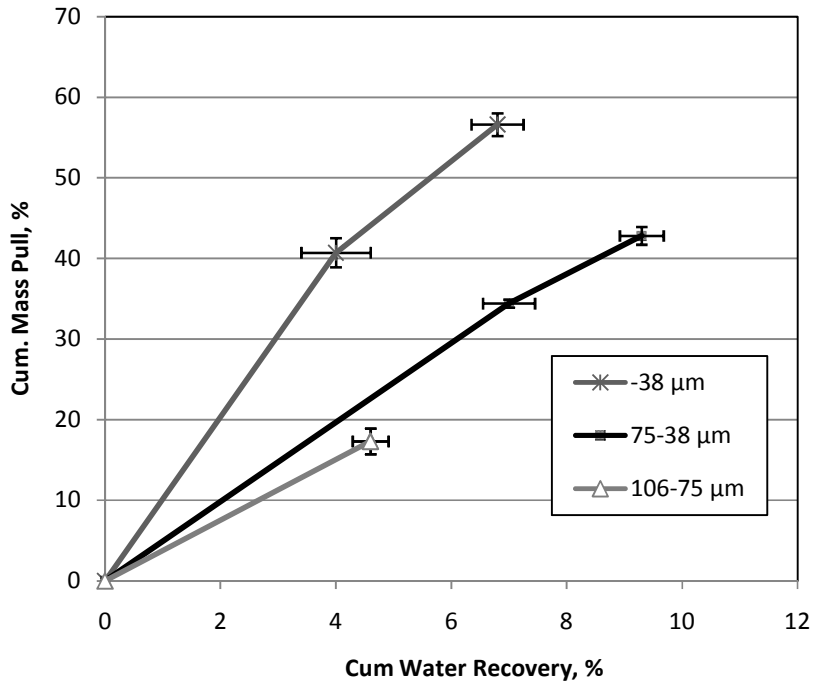

Figure 6.16: Cumulative mass pull versus cumulative water recovery under NHR of samples of varying PSDs.

On another note, this investigation shows that the natural hydrophobic response could still be observed at the coarser size of +75 −106 µm. From Figures 6.14 mass pull can be seen to be least at this size fraction. The total number of particles was much less and particle bubble collision efficiency was very low, so that mass pull stagnated after a little pull (18%).

Although the coarser size fraction also showed natural hydrophobic response, the absence of the fines required to stabilise the froth was obvious. The dynamic froth stability was much lower relative to the finer sizes, as indicated by the froth height in the cell (compare Figure A2.2 to Figure A2.7 in Appendix 2). The lower pull and the heavier coarser sizes also minimised entrapment (as mentioned) and coarser particles would also be more difficult to drag along. Only froth phase particles would, therefore, have best chances of making it to the launder. This gave rise to the high reverse recovery observed: Pd gave a notable recovery of 99 %. Many other metals gave between 98 and 97. However, enrichment was minimal, as the bulk of the feed was still left over as the concentrate under the prevailing kinetics. Using different kinetics to enhance higher mass pull will achieve a cleaner sink. The tradeoff in recovery will depend on how favourable the kinetics regime will be. In all, it can be said that this scheme will work, even for this larger size fraction.

6.4 CONCLUSION

It was projected that the particles in the PCB, being so diverse, some should exhibit natural hydrophobicity and this could be exploitable for a froth flotation scheme. The natural hydrophobic response was first observed under microflotation and then investigated in detail with the Leeds cell as reverse flotation with respect to the metallic values. It was also projected that enrichment versus recovery to the sink under this scheme could be optimised with variation in the operating kinetic regimes. The range of kinetic parameters appropriate for flotation application with this sample was observed. Most of the target metallic values wet and preferentially remained in the sink, justifying the reverse flotation approach. Au and Pd, which are the major economic drivers of PCB processing, were among the elements best enriched into the sink at optima of 64% for Au at an enrichment ratio above three. Ti achieved an even better performance. For these metals, which show preference for the sink, recovery loss to the float was observed to increase with mass pull, and not water recovery, when flotation results over varying

PSDs were compared. Such loss will therefore be due more to carry-over under bulk upward mass transfer and entrapment in the froth. Flotation over narrower size distribution still shows improvement in the performance obtained for the −75+38 µm size fraction, compared to the −75 µm wider PSD.

The results provide the basis to consider froth flotation as applicable for PCB CF beneficiation, and the natural hydrophobic response scheme to be effective in this regard.